

IMECE2007-41279

FULL SHEET CONTROL THROUGH THE USE OF STEER-ABLE NIPS

Edgar I. Ergueta

University of California
Berkeley, California 94720
Email: eergueta@me.berkeley.edu

Rene E. Sanchez

University of California
Berkeley, California 94720
Email: r2sanchez@gmail.com

Roberto Horowitz

University of California
Berkeley, California 94720
Email: horowitz@me.berkeley.edu

Masayoshi Tomizuka

University of California
Berkeley, California 94720
Email: tomizuka@me.berkeley.edu

ABSTRACT

State of the art high speed color printers require sheets being accurately positioned as they arrive to the image transfer station (ITS). This goal has been achieved by constructing and building a steerable nips mechanism, which is located upstream from the ITS. This mechanism consists of two rollers which not only rotate to advance the paper along the track, but also steer the paper in the yaw direction. This paper presents the design, experimental setup, system model, and the control law necessary to precisely correct for the lateral and angular positions of the sheet as well as to deliver it on time to the ITS. The system model is nonlinear and subject to four nonholonomic constraints. The control strategy used is based on linearization by state feedback with the addition of internal loops for the control of the process direction velocity and steering position of the rollers. This paper also provides a formal convergence analysis for the controller designed as well as the methodology required to tune it. The success of this mechatronic approach is corroborated through simulation and experimental results, which show that the controller is able to correct sheet errors under the condition that the page has nonzero initial and final longitudinal velocities.

1 INTRODUCTION

State of the art paper path control currently requires the sheets to be accurately positioned as they arrive to the image transfer station (ITS). This is achieved by using a registration device, which not only corrects for longitudinal, lateral and angular errors, but also delivers the sheet on time to the ITS. However, current designs cannot correct position errors at high speeds or cannot do it without marking the page.

In this paper we present a mechatronic solution to this problem, which corrects for errors at high speeds without damaging the sheet. This is achieved by using the steerable nips device depicted in Fig. 1 (US Patent Number 6,634,521).

The problem of controlling paper trajectories with steerable nips is similar to the control of two-wheel robots, such as the one studied in [1]. However, not only the two-wheel robot has one less degree of freedom, but also the control law proposed by the authors fails to account for singularities that arise when the steering angle of the wheels approaches zero. Also, in the case of the two-wheel robot, three inputs are needed to follow a reference trajectory. This is not the case with steerable nips, where four inputs are needed due to the flexibility of the paper; two inputs rotate and steer roller 1, whereas the other two inputs do the same for roller 2 (see Fig. 1).

Similar to the two-wheel robot, the steerable nips mechanism is a nonlinear system with four nonholonomic constraints.

These constraints come from non slip conditions on the rollers, and local velocities (of the paper) being zero in the direction perpendicular to the rotation of the rollers. Additional details on the constraints of this particular system can be found in [2].

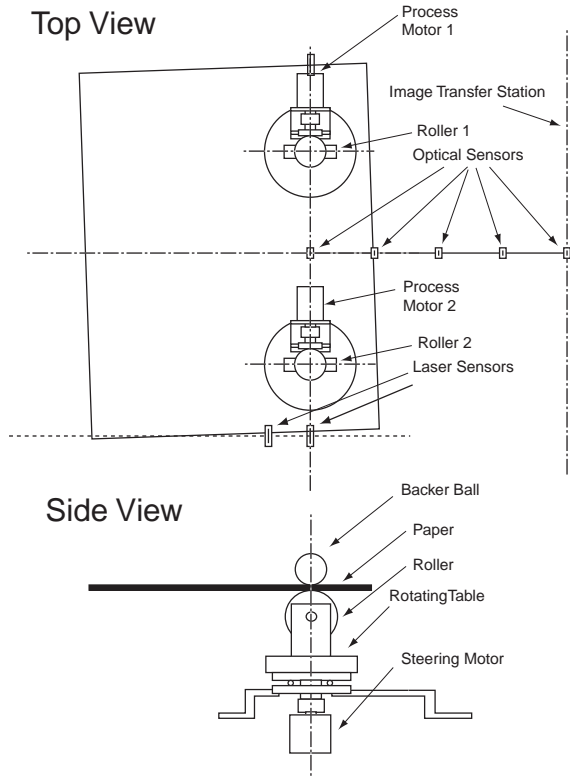


Figure 1. Schematic of Steerable Nips Fixture

The control objective of the steerable nips device consists of correcting the position of the sheet on a horizontal plane with the sheet moving in the longitudinal direction at all times. Since the page should move without getting damaged, it is also necessary to control the sheet's amount of buckling. The control strategy used to achieve these goals is based on state feedback linearization [3] with inner loops for the control of the roller's rotational angular velocity and steering angular position.

The remainder of this paper is organized as follows. Sections 2 and 3 describe the design of the steerable nips mechanism and the experimental setup, respectively. Section 4 presents the kinematic and dynamic model of the system. Sections 5 and 6 describe the control strategy and convergence analysis for a simplified system and for the system implemented, respectively. Simulation and experimental results are also shown. Finally, conclusions are stated in Section 7.

2 STEER-ABLE NIPS MECHANISM DESIGN

The steerable nips mechanism has been designed so that it can correct for lateral errors without having to move the actuators and without inflicting any damage on the paper. This has been achieved by steering two rollers, which are underneath a backer ball, as seen in Fig. 2. As a result, each roller is in contact with the sheet at only one point, letting the sheets safely move laterally while they are being driven forward. The roller is driven by a servo motor (*process direction motor*) attached to a rotating table, which is in turn steered by another servo motor (*steering motor*) through a coupling as shown in Fig. 2.

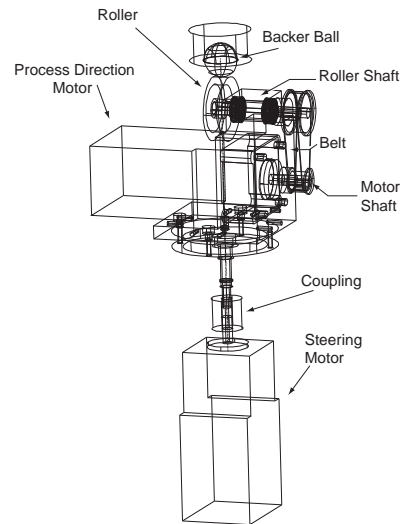


Figure 2. Process Direction Actuator and Steering Motor Mechanism

3 EXPERIMENTAL SETUP

As it can be seen in Fig. 3 the steerable nips mechanism is located below the horizontal plate where the page moves. A page is delivered to this mechanism by a feeder unit and it is removed from it by an exit roller. For practical purposes, we would like to correct the position of the sheet as it arrives to the exit roller.

In order to determine the position, orientation, and the amount of buckling of the sheet, it is required to detect the edges of the page. As seen in Fig. 1, two laser sensors are located on the right hand side of the page to measure the lateral and angular positions of the page. Furthermore, to measure the longitudinal position of the page, five single photodiode sensors, spaced 52mm apart, are located along the process direction. It should be noticed that whereas we are able to obtain continuous measurements for lateral and angular positions, we need to estimate the longitudinal position of the sheet between sensors and the amount of buckling

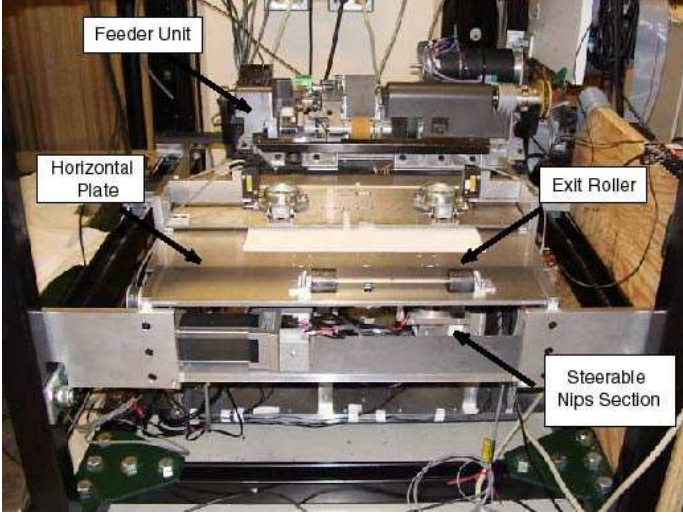


Figure 3. Experimental Setup

through the use of an observer. For this paper we have implemented an open-loop observer based on the kinematic relations described in the following section.

4 KINEMATICS AND DYNAMIC MODEL OF THE STEER-ABLE NIPS MECHANISM

Figure 4 represents a sheet while it is being tracked in the direction of the arrow labeled y ; the horizontal plate is not shown in this figure for clarity purposes. The leading right corner of the sheet, point C , will be used to track the position of the page.

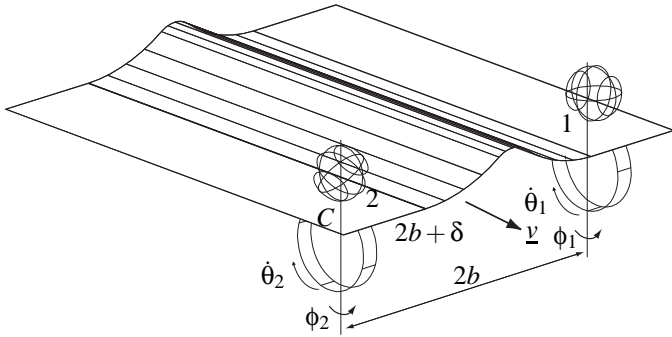


Figure 4. Steerable Nips with Paper Buckle

4.1 Notation

Figure 5 shows a schematic representation of the model variables for the steerable nips mechanism. This system has two independent steering rollers, located at points 1 and 2, which are separated by a distance $2b$. The space-fixed coordinates of the system (x, y, ϕ, δ) locate the leading right corner of the sheet

(point C), where x and y are the lateral and longitudinal position, respectively, ϕ is the angular position, and δ is the amount of buckling along the sheet, which is the difference between the distance separating points 1 and 2, as measured along the paper ($2b + \delta$) and along the straight line ($2b$), as shown in Fig. 4. Variables $(\theta_1, \theta_2, \phi_1, \phi_2)$ are coordinates at the actuator level (rollers); whereas θ_i represents the angular position of roller i in the direction parallel to the sheet, ϕ_i represents its angular position in the direction perpendicular to the sheet.

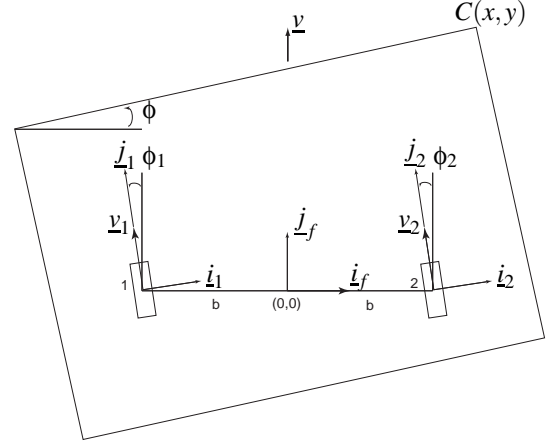


Figure 5. Schematic of Sheet and Roller from Top

4.2 Kinematics

The kinematic model of the system is derived so that the four nonholonomic constraints mentioned in Section 1 are satisfied at all times. This model, whose complete derivation can be found in [4], is represented by the following equations:

$$\dot{x} = r_1 \left(\sin \phi_1 - \frac{y}{2b + \delta} \cos \phi_1 \right) \dot{\theta}_1 + \frac{r_2 y}{2b + \delta} \cos \phi_2 \dot{\theta}_2 \quad (1)$$

$$\dot{y} = r_1 \cos \phi_1 \left(\frac{x + b}{2b + \delta} - 1 \right) \dot{\theta}_1 - \frac{r_2 (x + b)}{2b + \delta} \cos \phi_2 \dot{\theta}_2 \quad (2)$$

$$\dot{\phi} = \frac{1}{2b + \delta} (r_1 \cos \phi_1 \dot{\theta}_1 - r_2 \cos \phi_2 \dot{\theta}_2) \quad (3)$$

$$\dot{\delta} = r_2 \sin \phi_2 \dot{\theta}_2 - r_1 \sin \phi_1 \dot{\theta}_1 \quad (4)$$

4.3 Actuator Dynamics

Assuming that the belt connecting the process direction motor to the roller is very stiff (Fig. 2) and that the motor inductance is sufficiently low, we can obtain the following simple model for the process direction actuator dynamics:

$$\ddot{\theta}_i + \alpha_{pi} \dot{\theta}_i = \beta_{pi} V_{pi}; \quad (i = 1, 2) \quad (5)$$

where V_{pi} is the voltage input to the motor, and α_{pi} and β_{pi} depend on the inertias and rotational viscous damping coefficients of the different components shown in Fig. 2 as well as on the resistance and torque constant of the motor; subindex i refers to each of the two process direction motors.

Similarly, we can obtain the following model for the steering actuator dynamics:

$$\ddot{\phi}_i + \alpha_{si}\dot{\phi}_i = \beta_{si}V_{si}; \quad (i = 1, 2) \quad (6)$$

where V_{si} , α_{si} and β_{si} are defined as in the previous case.

4.4 Dynamic System Model

Letting $\underline{x} = [x \ y \ \phi \ \delta \ \dot{x} \ \dot{y} \ \dot{\phi} \ \dot{\delta}]^T$ be the state vector and $\underline{y} = [x \ y \ \phi \ \delta]^T$ be the output vector, differentiating Eqs. (1)-(4), and using Eqs. (5) and (6) for both process direction motors and both steering motors, respectively, we obtain the following dynamic system model:

$$\underline{\dot{y}} = m(\underline{x}) + N(\underline{x}) \begin{bmatrix} \ddot{\theta}_1 \\ \ddot{\theta}_2 \\ \ddot{\phi}_1 \\ \ddot{\phi}_2 \end{bmatrix} \quad (7)$$

$$\ddot{\theta}_1 + \alpha_{p1}\dot{\theta}_1 = \beta_{p1}u_1 \quad (8)$$

$$\ddot{\theta}_2 + \alpha_{p2}\dot{\theta}_2 = \beta_{p2}u_2 \quad (9)$$

where $m(\underline{x})$ is a 4×1 vector and $N(\underline{x})$ is a 4×4 matrix, both of which depend nonlinearly on the system states.

5 CONTROL STRATEGY AND CONVERGENCE ANALYSIS FOR A SIMPLIFIED SYSTEM

Before engaging into the analysis of the system implemented experimentally, we should look into a simplified case for two main reasons. First, it will facilitate the understanding of the controller developed for the implemented system, since the controller synthesis for both the simplified and implemented systems undergo similar steps although the latter has a higher degree of complexity. Secondly, some of the controller gains obtained for the simplified system will serve as initial points for tuning the controller of the implemented system.

Let us then consider the case for which the input voltages to the process motors are two of the four system inputs, u_1 and u_2 , but the other two inputs, u_3 and u_4 , are the steering angular velocities. Thus, Eqs. (9) reduce to

$$\begin{aligned} \dot{\phi}_1 &= u_3 \\ \dot{\phi}_2 &= u_4 \end{aligned} \quad (10)$$

5.1 Control Strategy

The block diagram for this simplified case is shown in Fig.6.

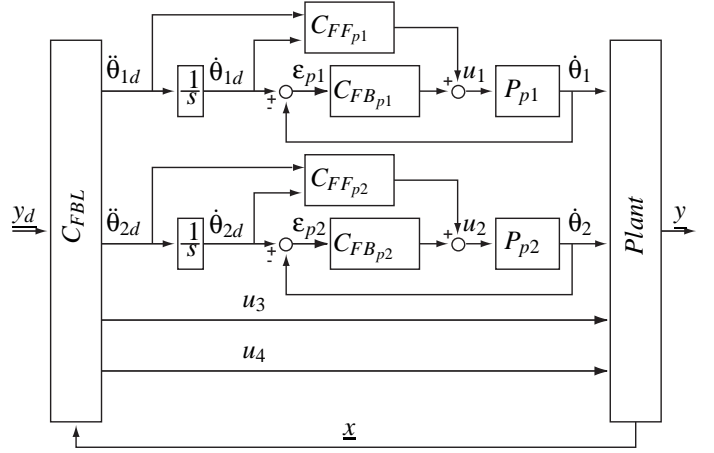


Figure 6. System Block Diagram for Simplified System

Here, the *Plant* is represented by Eq. (7) and P_{p1} and P_{p2} by Eqs. (8). Furthermore, the nonlinear feedback control law, C_{FBL} , is based on feedback linearization [5]:

$$\begin{bmatrix} \ddot{\theta}_{1d} \\ \ddot{\theta}_{2d} \\ u_3 \\ u_4 \end{bmatrix} = N^{-1}(\underline{x})(\underline{y} - m(\underline{x})) \quad (11)$$

Whereas two of the inputs to the plant, u_3 and u_4 , are obtained from the feedback linearization control law, the other two, u_1 and u_2 , are generated by a feedback plus feedforward control strategy used for velocity control of the process direction motors:

$$C_{FBpi}(s) = \eta_{pi} + \frac{\gamma_{pi}}{s}; \quad C_{FFpi}(s) = \frac{1}{\beta_{pi}}(1 + \frac{\alpha_{pi}}{s}); \quad (i = 1, 2) \quad (12)$$

where η_{pi} and γ_{pi} are the PI controller gains, and α_{pi} and β_{pi} are defined in Eq. (8) for $i = 1, 2$. The success of this control strategy depends on the invertibility of matrix $N(x)$. In [4] it is shown that this matrix is invertible as long as the sheet is always moving in the longitudinal direction. Also notice that for the nonlinear part of the system, Eq. (7), since each of the four outputs has a relative degree of 2, the zero dynamics is of dimension zero.

5.2 Convergence Analysis of Closed-Loop System

Let us first note that the process actuator errors are defined by

$$\varepsilon_{pi} = \dot{\theta}_{id} - \dot{\theta}_i; \quad (i = 1, 2) \quad (13)$$

and thus we can combine Eqs. (7), (11) and (13) to obtain

$$\underline{\dot{y}} = \underline{y} - N(\underline{x}) \begin{bmatrix} \dot{\varepsilon}_{p1} \\ \dot{\varepsilon}_{p2} \\ 0 \\ 0 \end{bmatrix} \quad (14)$$

If we further let \underline{v} be

$$\underline{v} = \begin{pmatrix} v_1 \\ v_2 \\ v_3 \\ v_4 \end{pmatrix} = \begin{pmatrix} \dot{x}_d + (K_x + \lambda_x)\dot{\tilde{x}} + K_x\lambda_x\tilde{x} \\ \dot{y}_d + (K_y + \lambda_y)\dot{\tilde{y}} + K_y\lambda_y\tilde{y} \\ \dot{\phi}_d + (K_\phi + \lambda_\phi)\dot{\tilde{\phi}} + K_\phi\lambda_\phi\tilde{\phi} \\ \dot{\delta}_d + (K_\delta + \lambda_\delta)\dot{\tilde{\delta}} + K_\delta\lambda_\delta\tilde{\delta} \end{pmatrix} \quad (15)$$

where paper coordinate errors are defined by

$$\begin{aligned} \tilde{x} &= x_d - x; & \tilde{y} &= y_d - y \\ \tilde{\phi} &= \phi_d - \phi; & \tilde{\delta} &= \delta_d - \delta \end{aligned} \quad (16)$$

then from Eq. (14) we can see that if $\dot{\varepsilon}_{p1}$ and $\dot{\varepsilon}_{p2}$ tend to zero, then x , y , ϕ , and δ will converge asymptotically to x_d , y_d , ϕ_d , and δ_d , respectively.

In order to show the converge of this control strategy let us also define the following surface errors:

$$\begin{aligned} s_x &= \dot{\tilde{x}} + \lambda_x\tilde{x}; & s_y &= \dot{\tilde{y}} + \lambda_y\tilde{y} \\ s_\phi &= \dot{\tilde{\phi}} + \lambda_\phi\tilde{\phi}; & s_\delta &= \dot{\tilde{\delta}} + \lambda_\delta\tilde{\delta} \\ s_{\varepsilon_{p1}} &= \dot{\varepsilon}_{p1} + \lambda_{\varepsilon_{p1}}\varepsilon_{p1}; & s_{\varepsilon_{p2}} &= \dot{\varepsilon}_{p2} + \lambda_{\varepsilon_{p2}}\varepsilon_{p2}; \end{aligned} \quad (17)$$

Expressing \underline{v} in term of the surface errors and letting γ_{p1} and γ_{p2} be defined by

$$\gamma_{pi} = \frac{(\alpha_{pi} + \beta_{pi}\eta_{pi} - \lambda_{\varepsilon_{pi}})\lambda_{\varepsilon_{pi}}}{\beta_{pi}}; \quad (i = 1, 2) \quad (18)$$

the time derivatives of the errors above mentioned (Eqs. (13), (16), and (17)) can be expressed as:

$$\begin{aligned} \dot{\tilde{x}} &= -\lambda_x\tilde{x} + s_x \\ \dot{\tilde{y}} &= -\lambda_y\tilde{y} + s_y \\ \dot{\tilde{\phi}} &= -\lambda_\phi\tilde{\phi} + s_\phi \\ \dot{\tilde{\delta}} &= -\lambda_\delta\tilde{\delta} + s_\delta \\ \dot{\varepsilon}_{p1} &= -\lambda_{\varepsilon_{p1}}\varepsilon_{p1} + s_{\varepsilon_{p1}} \\ \dot{\varepsilon}_{p2} &= -\lambda_{\varepsilon_{p2}}\varepsilon_{p2} + s_{\varepsilon_{p2}} \\ \dot{s}_x &= -K_x s_x + n_{11}\dot{\varepsilon}_{p1} + n_{12}\dot{\varepsilon}_{p2} \\ \dot{s}_y &= -K_y s_y + n_{21}\dot{\varepsilon}_{p1} + n_{22}\dot{\varepsilon}_{p2} \\ \dot{s}_\phi &= -K_\phi s_\phi + n_{31}\dot{\varepsilon}_{p1} + n_{32}\dot{\varepsilon}_{p2} \\ \dot{s}_\delta &= -K_\delta s_\delta + n_{41}\dot{\varepsilon}_{p1} + n_{42}\dot{\varepsilon}_{p2} \\ \dot{s}_{\varepsilon_{p1}} &= -(\alpha_{p1} + \beta_{p1}\eta_{p1} - \lambda_{\varepsilon_{p1}})s_{\varepsilon_{p1}} \\ \dot{s}_{\varepsilon_{p2}} &= -(\alpha_{p2} + \beta_{p2}\eta_{p2} - \lambda_{\varepsilon_{p2}})s_{\varepsilon_{p2}} \end{aligned} \quad (19)$$

where n_{ij} ($i = 1, 2, 3, 4; j = 1, 2$) are elements of the first two columns of matrix $N(x)$.

If we define the desired trajectory by

$$(x_d, y_d, \phi_d, \delta_d, \dot{x}_d, \dot{y}_d, \dot{\phi}_d, \dot{\delta}_d) = (0, vt, 0, 0, 0, v, 0, 0) \quad (20)$$

where v is the nominal longitudinal velocity of the sheet, and we linearize the system described in Eq. (19) around $\tilde{x} = \tilde{y} = \tilde{\phi} = \tilde{\delta} = \varepsilon_{p1} = \varepsilon_{p2} = s_x = s_y = s_\phi = s_\delta = s_{\varepsilon_{p1}} = s_{\varepsilon_{p2}} = 0$, we can obtain an expression of the form

$$\dot{\underline{e}}(t) = G(t)\underline{e}(t) \quad (21)$$

where $\underline{e}(t)$ is defined as

$$\underline{e}(t) = (\bar{x} \ \bar{y} \ \bar{\phi} \ \bar{\delta} \ \bar{\varepsilon}_{p1} \ \bar{\varepsilon}_{p2})^T \quad (22)$$

and $G(t)$ is given by

$$G(t) = \begin{pmatrix} A_x & 0 & 0 & 0 & B_x^{\varepsilon_{p1}}(t) & B_x^{\varepsilon_{p2}}(t) \\ 0 & A_y & 0 & 0 & B_y^{\varepsilon_{p1}} & B_y^{\varepsilon_{p2}} \\ 0 & 0 & A_\phi & 0 & B_\phi^{\varepsilon_{p1}} & B_\phi^{\varepsilon_{p2}} \\ 0 & 0 & 0 & A_\delta & 0 & 0 \\ 0 & 0 & 0 & 0 & A_{\varepsilon_{p1}} & 0 \\ 0 & 0 & 0 & 0 & 0 & A_{\varepsilon_{p2}} \end{pmatrix} \quad (23)$$

The elements of vector $\underline{e}(t)$ in Eq. (22) are

$$\begin{aligned} \bar{x} &= \begin{pmatrix} \tilde{x} \\ s_x \end{pmatrix}, & \bar{y} &= \begin{pmatrix} \tilde{y} \\ s_y \end{pmatrix}, & \bar{\phi} &= \begin{pmatrix} \tilde{\phi} \\ s_\phi \end{pmatrix} \\ \bar{\delta} &= \begin{pmatrix} \tilde{\delta} \\ s_\delta \end{pmatrix}, & \bar{\varepsilon}_{p1} &= \begin{pmatrix} \varepsilon_{p1} \\ s_{\varepsilon_{p1}} \end{pmatrix}, & \bar{\varepsilon}_{p2} &= \begin{pmatrix} \varepsilon_{p2} \\ s_{\varepsilon_{p2}} \end{pmatrix} \end{aligned} \quad (24)$$

and the matrix components of $G(t)$ in Eq. (23) are

$$\begin{aligned} A_x &= \begin{pmatrix} -\lambda_x & 1 \\ 0 & -K_x \end{pmatrix}, & A_y &= \begin{pmatrix} -\lambda_y & 1 \\ 0 & -K_y \end{pmatrix} \\ A_\phi &= \begin{pmatrix} -\lambda_\phi & 1 \\ 0 & -K_\phi \end{pmatrix}, & A_\delta &= \begin{pmatrix} -\lambda_\delta & 1 \\ 0 & -K_\delta \end{pmatrix} \\ A_{\varepsilon_{p1}} &= \begin{pmatrix} -\lambda_{\varepsilon_{p1}} & 1 \\ 0 & -g_{10,10} \end{pmatrix}, & A_{\varepsilon_{p2}} &= \begin{pmatrix} -\lambda_{\varepsilon_{p2}} & 1 \\ 0 & -g_{12,12} \end{pmatrix} \\ B_x^{\varepsilon_{p1}}(t) &= \begin{pmatrix} 0 & 0 \\ g_{2,9} & g_{2,10} \end{pmatrix}, & B_x^{\varepsilon_{p2}}(t) &= \begin{pmatrix} 0 & 0 \\ g_{2,11} & g_{2,12} \end{pmatrix} \\ B_y^{\varepsilon_{p1}} &= \begin{pmatrix} 0 & 0 \\ g_{4,9} & g_{4,10} \end{pmatrix}, & B_y^{\varepsilon_{p2}} &= \begin{pmatrix} 0 & 0 \\ g_{4,11} & g_{4,12} \end{pmatrix} \\ B_\phi^{\varepsilon_{p1}} &= \begin{pmatrix} 0 & 0 \\ g_{6,9} & g_{6,10} \end{pmatrix}, & B_\phi^{\varepsilon_{p2}} &= \begin{pmatrix} 0 & 0 \\ g_{6,11} & g_{6,12} \end{pmatrix} \end{aligned} \quad (25)$$

Elements $g_{i,j}$, above, depend on system parameters and the controller gains. Elements $g_{2,9}$, $g_{2,10}$, $g_{2,11}$, and $g_{2,12}$ depend explicitly on time, and they do so linearly. This dependence on time comes from the desired trajectory of the sheet shown in Eq. (20).

From Eqs. (21)-(25) we can obtain the following expressions

$$\begin{aligned} \dot{\tilde{x}} &= A_x\bar{x} + B_x^{\varepsilon_{p1}}(t)\bar{\varepsilon}_{p1} + B_x^{\varepsilon_{p2}}(t)\bar{\varepsilon}_{p2} \\ \dot{\tilde{y}} &= A_y\bar{y} + B_y^{\varepsilon_{p1}}\bar{\varepsilon}_{p1} + B_y^{\varepsilon_{p2}}\bar{\varepsilon}_{p2} \\ \dot{\tilde{\phi}} &= A_\phi\bar{\phi} + B_\phi^{\varepsilon_{p1}}\bar{\varepsilon}_{p1} + B_\phi^{\varepsilon_{p2}}\bar{\varepsilon}_{p2} \\ \dot{\tilde{\delta}} &= A_\delta\bar{\delta} \\ \dot{\varepsilon}_{p1} &= A_{\varepsilon_{p1}}\bar{\varepsilon}_{p1} \\ \dot{\varepsilon}_{p2} &= A_{\varepsilon_{p2}}\bar{\varepsilon}_{p2} \end{aligned} \quad (26)$$

We can easily solve for $\bar{\delta}(t)$, $\bar{\epsilon}_{p1}(t)$, and $\bar{\epsilon}_{p2}(t)$ from Eq. (26):

$$\begin{aligned}\bar{\delta}(t) &= e^{A_\delta t} \bar{\delta}(0) \\ \bar{\epsilon}_{p1}(t) &= e^{A_{\epsilon_{p1}} t} \bar{\epsilon}_{p1}(0) \\ \bar{\epsilon}_{p2}(t) &= e^{A_{\epsilon_{p2}} t} \bar{\epsilon}_{p2}(0)\end{aligned}\quad (27)$$

Finally, using Eqs. (26) and (27), the solutions for $\bar{x}(t)$, $\bar{y}(t)$, and $\bar{\phi}(t)$ are given by

$$\begin{aligned}\bar{x}(t) &= e^{A_x t} \bar{x}(0) + \left[\int_0^t e^{A_x(t-\tau)} B_x^{\epsilon_{p1}}(\tau) e^{A_{\epsilon_{p1}} \tau} d\tau \right] \bar{\epsilon}_{p1}(0) \\ &\quad + \left[\int_0^t e^{A_x(t-\tau)} B_x^{\epsilon_{p2}}(\tau) e^{A_{\epsilon_{p2}} \tau} d\tau \right] \bar{\epsilon}_{p2}(0) \\ \bar{y}(t) &= e^{A_y t} \bar{y}(0) + \left[\int_0^t e^{A_y(t-\tau)} B_y^{\epsilon_{p1}}(\tau) e^{A_{\epsilon_{p1}} \tau} d\tau \right] \bar{\epsilon}_{p1}(0) \\ &\quad + \left[\int_0^t e^{A_y(t-\tau)} B_y^{\epsilon_{p2}}(\tau) e^{A_{\epsilon_{p2}} \tau} d\tau \right] \bar{\epsilon}_{p2}(0) \\ \bar{\phi}(t) &= e^{A_\phi t} \bar{\phi}(0) + \left[\int_0^t e^{A_\phi(t-\tau)} B_\phi^{\epsilon_{p1}}(\tau) e^{A_{\epsilon_{p1}} \tau} d\tau \right] \bar{\epsilon}_{p1}(0) \\ &\quad + \left[\int_0^t e^{A_\phi(t-\tau)} B_\phi^{\epsilon_{p2}}(\tau) e^{A_{\epsilon_{p2}} \tau} d\tau \right] \bar{\epsilon}_{p2}(0)\end{aligned}\quad (28)$$

It should be noticed that even though the solutions for $\bar{x}(t)$, $\bar{y}(t)$, and $\bar{\phi}(t)$ involve convolution integrals, these can easily be solved algebraically. In fact, this is true even for the case of $\bar{x}(t)$, due to the linear nature of the time-dependent terms in $B_x^{\epsilon_{p1}}(t)$ and $B_x^{\epsilon_{p2}}(t)$.

Furthermore, we can see from Eqs. (25), (27) and (28) that by proper selection of the controller gains we can make matrices A_x , A_y , A_ϕ , A_δ , $A_{\epsilon_{p1}}$, and $A_{\epsilon_{p2}}$ Hurwitz, and thus we can make the solutions $\bar{x}(t)$, $\bar{y}(t)$, $\bar{\phi}(t)$, $\bar{\delta}(t)$, $\bar{\epsilon}_{p1}(t)$, and $\bar{\epsilon}_{p2}(t)$ converge.

5.3 Controller Design Methodology

The control specifications are as follows:

- i. The sheet has finite dimensions and moves with a nominal longitudinal velocity, v .
- ii. The distance between the first and last optical sensors in Fig. 1 is given by L . Thus, the leading edge of the sheet will exit the stear-able nips section at time $T = L/v$.
- iii. The sheet has initial maximum errors $|\bar{x}(0)|$, $|\bar{y}(0)|$, $|\bar{\phi}(0)|$, and $|\bar{\delta}(0)|$ (as in Table 1).
- iv. The error at time T , when the sheet exits the nips section, must be smaller than or equal to $|\bar{x}(T)|$, $|\bar{y}(T)|$, $|\bar{\phi}(T)|$, and $|\bar{\delta}(T)|$ (as in Table 1).

Now, by looking at the first expression in Eqs. (27) and the definition of A_δ in Eq. (25), we can see that, for a page of finite dimensions moving at a given nominal longitudinal velocity, we can easily obtain the controller gains, λ_δ and K_δ , required to reduce the error, $\bar{\delta}$, from $\bar{\delta}(0)$ to $\bar{\delta}(T)$. We can similarly obtain the rest of the controller gains using the remaining expressions in Eqs. (27) and Eqs. (28).

Initial Errors	Final Errors
$ \bar{x}(0) \leq 0.008 \text{ m}$	$ \bar{x}(T) \leq 0.0013 \text{ m}$
$ \bar{y}(0) \leq 0.040 \text{ m}$	$ \bar{y}(T) \leq 0.0016 \text{ m}$
$ \bar{\phi}(0) \leq 0.025 \text{ rad}$	$ \bar{\phi}(T) \leq 0.0035 \text{ rad}$
$ \bar{\delta}(0) \leq 0.0001 \text{ m}$	$ \bar{\delta}(T) \leq 0.00002 \text{ m}$

Table 1. Initial and Final State Errors for Simulation Tests

Thus, based on the control specifications just mentioned, we can use the following procedure, which summarizes the steps required to obtain all controller gains:

- i. Determine gains $(\lambda_\delta, K_\delta)$, $(\lambda_{\epsilon_{p1}}, \eta_{p1})$, and $(\lambda_{\epsilon_{p2}}, \eta_{p2})$ from each of the three expressions in Eqs. (27), respectively.
- ii. Once the gains from step (i) have been obtained, determine gains (λ_x, K_x) , (λ_y, K_y) , and (λ_ϕ, K_ϕ) from each of the three expressions in Eqs. (28), respectively.

5.4 Simulation Results

In order to determine the efficacy of the controller described above we performed simulation tests. The goal was to take a letter-sized sheet moving at a nominal longitudinal velocity of 0.5 m/s from the initial to the final state errors shown in Table 1. Based on the procedure presented in Section 5.3 and the initial and final errors shown in Table 1 the following controller gains were obtained:

$$\begin{aligned}(\lambda_x, K_x) &= (80, 4.5); & (\lambda_y, K_y) &= (80, 8.0) \\ (\lambda_\phi, K_\phi) &= (80, 4.9); & (\lambda_\delta, K_\delta) &= (100, 3.9) \\ (\lambda_{\epsilon_{p1}}, \eta_{p1}) &= (100, 0.26); & (\lambda_{\epsilon_{p2}}, \eta_{p2}) &= (100, 0.26)\end{aligned}$$

As we can see in Fig. 7, the controller gains effectively corrects the position of the sheet within 0.42 seconds.

6 CONTROL STRATEGY AND CONVERGENCE ANALYSIS FOR THE SYSTEM IMPLEMENTED

Contrarily to the simplified system in Section 5, when designing the controller for the actual setup, the steering actuator dynamics, as defined in Eqs. (9), must be taken into account. Due to these extra dynamics the control strategy becomes more involved, since we now need to control locally the position of the steering motors. As we will see in Section 6.3, even though the methodology to obtain the controller gains is not as direct as in the simplified system, controller gains can still be easily obtained after a couple of iterations.

6.1 Control Strategy

The block diagram of the control system is shown in Fig.8.

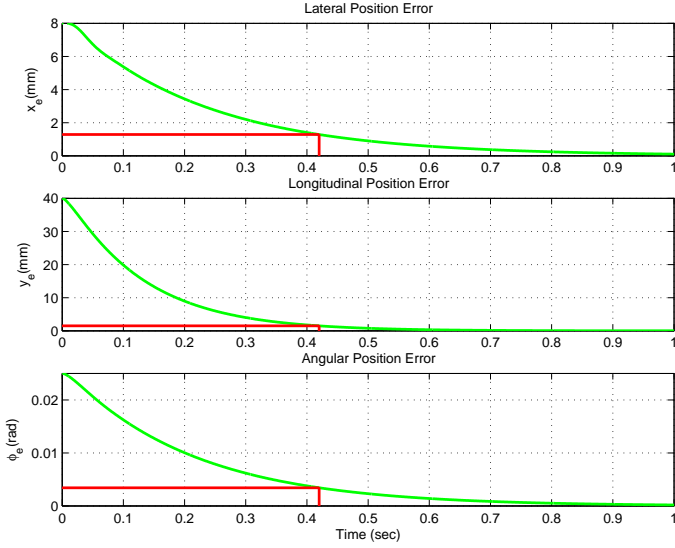


Figure 7. Simulation Results for the Simplified System

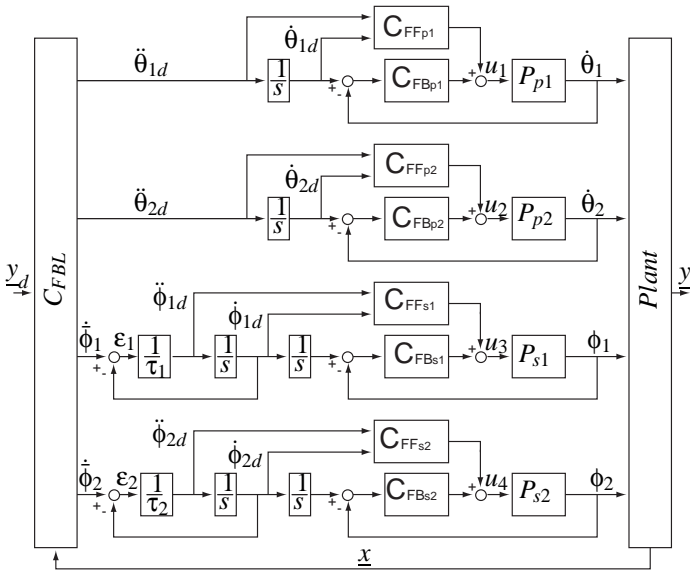


Figure 8. System Block Diagram for Implemented System

As in the simplified case, the *Plant*, the process direction motors P_{p1} and P_{p2} , the nonlinear feedback control law, C_{FBL} , and the feedback and feedforward controllers for the process motors are given by Eqs. (7), (8), (11) and (12), respectively. This time the plant for the steering motors, P_{s1} and P_{s2} are given by Eqs. (9). Furthermore, the position of the steering actuators is controlled by a feedback plus feedforward control strategy given by:

$$C_{FB_{si}}(s) = \eta_{si} + \gamma_{pi}s; \quad C_{FF_{si}}(s) = \frac{1}{\beta_{si}} \left(1 + \frac{\alpha_{si}}{s}\right); \quad (i = 1, 2) \quad (29)$$

where η_{si} and γ_{si} are the PD controller gains, and α_{si} and β_{si} are defined in Eqs. (9) for $i = 1, 2$. As shown in Fig. 8, in order to use feedforward control, we need to generate the steering acceleration estimate, $\ddot{\phi}_{id}$, through the use of a first order filter with gain τ_i ($i = 1, 2$). Note that if τ_i is sufficiently small, the value of $\dot{\phi}_{id}$ will be very close to that of $\dot{\phi}_i$ for $i = 1, 2$.

6.2 Convergence Analysis of Closed-Loop System

The convergence analysis of the closed-loop system follows the same development as in Section 5.2. For instance, the process actuator errors are defined as in Eq. (13), the steering actuator errors are defined by

$$\varepsilon_{si} = \phi_{id} - \phi_i; \quad (i = 1, 2) \quad (30)$$

and the errors from the first order filter filters ε_i are defined by

$$\varepsilon_i = \dot{\phi}_i - \dot{\phi}_{id}; \quad (i = 1, 2) \quad (31)$$

We can now define \underline{v} as in Eq. (15) and the paper coordinate errors as in Eq. (16). Furthermore, in addition to the surface errors defined in Eq. (17), we should also define surface errors for the steering motors:

$$s_{\varepsilon_{s1}} = \dot{\varepsilon}_{s1} + \lambda_{\varepsilon_{s1}} \varepsilon_{s1}; \quad s_{\varepsilon_{s2}} = \dot{\varepsilon}_{s2} + \lambda_{\varepsilon_{s2}} \varepsilon_{s2} \quad (32)$$

Then, if we define γ_{p1} and γ_{p2} as in Eq. (18) and define η_{s1} and η_{s2} as

$$\eta_{si} = \frac{(\alpha_{si} + \gamma_{si}\beta_{si} - \lambda_{si})\lambda_{si}}{\beta_{si}} \quad (i = 1, 2) \quad (33)$$

by differentiating Eqs. (13), (16), (17), (30), (31), and (32) we obtain the following error dynamics:

$$\begin{aligned} \dot{\tilde{x}} &= -\lambda_x \tilde{x} + s_x \\ \dot{\tilde{y}} &= -\lambda_y \tilde{y} + s_y \\ \dot{\tilde{\phi}} &= -\lambda_\phi \tilde{\phi} + s_\phi \\ \dot{\tilde{\delta}} &= -\lambda_\delta \tilde{\delta} + s_\delta \\ \dot{\varepsilon}_{p1} &= -\lambda_{p1} \varepsilon_{p1} + s_{\varepsilon_{p1}} \\ \dot{\varepsilon}_{p2} &= -\lambda_{p2} \varepsilon_{p2} + s_{\varepsilon_{p2}} \\ \dot{\varepsilon}_{s1} &= -\lambda_{s1} \varepsilon_{s1} + s_{\varepsilon_{s1}} \\ \dot{\varepsilon}_{s2} &= -\lambda_{s2} \varepsilon_{s2} + s_{\varepsilon_{s2}} \end{aligned}$$

$$\begin{aligned} \dot{s}_x &= -K_x s_x + n_{11} \dot{\varepsilon}_{p1} + n_{12} \dot{\varepsilon}_{p2} + n_{13} (\dot{\varepsilon}_{s1} + \varepsilon_1) + n_{14} (\dot{\varepsilon}_{s2} + \varepsilon_2) \\ \dot{s}_y &= -K_y s_y + n_{21} \dot{\varepsilon}_{p1} + n_{22} \dot{\varepsilon}_{p2} + n_{23} (\dot{\varepsilon}_{s1} + \varepsilon_1) + n_{24} (\dot{\varepsilon}_{s2} + \varepsilon_2) \\ \dot{s}_\phi &= -K_\phi s_\phi + n_{31} \dot{\varepsilon}_{p1} + n_{32} \dot{\varepsilon}_{p2} + n_{33} (\dot{\varepsilon}_{s1} + \varepsilon_1) + n_{34} (\dot{\varepsilon}_{s2} + \varepsilon_2) \\ \dot{s}_\delta &= -K_\delta s_\delta + n_{41} \dot{\varepsilon}_{p1} + n_{42} \dot{\varepsilon}_{p2} + n_{43} (\dot{\varepsilon}_{s1} + \varepsilon_1) + n_{44} (\dot{\varepsilon}_{s2} + \varepsilon_2) \end{aligned}$$

$$\begin{aligned} \dot{s}_{\varepsilon_{p1}} &= -(\alpha_{p1} + \beta_{p1}\eta_{p1} - \lambda_{\varepsilon_{p1}}) s_{\varepsilon_{p1}} \\ \dot{s}_{\varepsilon_{p2}} &= -(\alpha_{p2} + \beta_{p2}\eta_{p2} - \lambda_{\varepsilon_{p2}}) s_{\varepsilon_{p2}} \\ \dot{s}_{\varepsilon_{s1}} &= -(\alpha_{s1} + \beta_{s1}\eta_{s1} - \lambda_{\varepsilon_{s1}}) s_{\varepsilon_{s1}} \\ \dot{s}_{\varepsilon_{s2}} &= -(\alpha_{s2} + \beta_{s2}\eta_{s2} - \lambda_{\varepsilon_{s2}}) s_{\varepsilon_{s2}} \end{aligned}$$

$$\begin{aligned} \dot{\varepsilon}_1 &= -\frac{1}{\tau_1} \varepsilon_1 + \frac{\delta \dot{\phi}_1}{\delta \Psi} \underline{\Psi} + \frac{\delta \dot{\phi}_1}{\delta t} \\ \dot{\varepsilon}_2 &= -\frac{1}{\tau_2} \varepsilon_2 + \frac{\delta \dot{\phi}_2}{\delta \Psi} \underline{\Psi} + \frac{\delta \dot{\phi}_2}{\delta t} \end{aligned}$$

$$(34)$$

where n_{ij} ($i,j=1,2,3,4$) are elements of matrix $N(\underline{x})$ and $\underline{\Psi}$ is defined by:

$$\underline{\Psi} = (\tilde{x} \ s_x \ \tilde{y} \ s_y \ \tilde{\phi} \ s_\phi \ \tilde{\delta} \ s_\delta)^T \quad (35)$$

Linearizing Eq. (34) around $\tilde{x} = \tilde{y} = \tilde{\phi} = \tilde{\delta} = \varepsilon_{p1} = \varepsilon_{p2} = \varepsilon_{s1} = \varepsilon_{s2} = s_x = s_y = s_\phi = s_\delta = s_{\varepsilon_{p1}} = s_{\varepsilon_{p2}} = s_{\varepsilon_{s1}} = s_{\varepsilon_{s2}} = \varepsilon_1 = \varepsilon_2 = 0$ we obtain an expression of the form

$$\dot{\underline{\varepsilon}}(t) = G(t)\underline{\varepsilon}(t) \quad (36)$$

where this time $\underline{\varepsilon}(t)$ is defined as

$$\underline{\varepsilon}(t) = (\bar{x} \ \bar{y} \ \bar{\phi} \ \bar{\delta} \ \bar{\varepsilon}_{p1} \ \bar{\varepsilon}_{p2} \ \bar{\varepsilon}_{s1} \ \bar{\varepsilon}_{s2} \ \bar{\varepsilon})^T \quad (37)$$

and $G(t)$ is given by

$$G(t) = \begin{pmatrix} A_x & 0 & 0 & 0 & B_x^{\varepsilon_{p1}}(t) & B_x^{\varepsilon_{p2}}(t) & B_x^{\varepsilon_{s1}} & 0 & B_x^{\varepsilon} \\ 0 & A_y & 0 & 0 & B_y^{\varepsilon_{p1}} & B_y^{\varepsilon_{p2}} & 0 & 0 & 0 \\ 0 & 0 & A_\phi & 0 & B_\phi^{\varepsilon_{p1}} & B_\phi^{\varepsilon_{p2}} & 0 & 0 & 0 \\ 0 & 0 & 0 & A_\delta & 0 & 0 & B_\delta^{\varepsilon_{s1}} & B_\delta^{\varepsilon_{s2}} & B_\delta^{\varepsilon} \\ 0 & 0 & 0 & 0 & A_{\varepsilon_{p1}} & 0 & 0 & 0 & 0 \\ 0 & 0 & 0 & 0 & 0 & A_{\varepsilon_{p2}} & 0 & 0 & 0 \\ 0 & 0 & 0 & 0 & 0 & 0 & A_{\varepsilon_{s1}} & 0 & 0 \\ 0 & 0 & 0 & 0 & 0 & 0 & 0 & A_{\varepsilon_{s2}} & 0 \\ B_\varepsilon^x & 0 & B_\varepsilon^\phi(t) & B_\varepsilon^\delta & B_\varepsilon^{\varepsilon_{p1}}(t) & B_\varepsilon^{\varepsilon_{p2}}(t) & B_\varepsilon^{\varepsilon_{s1}} & B_\varepsilon^{\varepsilon_{s2}} & A_\varepsilon \end{pmatrix} \quad (38)$$

Elements \bar{x} , \bar{y} , $\bar{\phi}$, $\bar{\delta}$, $\bar{\varepsilon}_{p1}$, and $\bar{\varepsilon}_{p2}$ in Eq. (37) are defined as in Eq. (24) and $\bar{\varepsilon}_{s1}$, $\bar{\varepsilon}_{s2}$, and $\bar{\varepsilon}$ are similarly defined by:

$$\begin{aligned} \bar{\varepsilon}_{s1} &= \begin{pmatrix} \varepsilon_{s1} \\ s_{\varepsilon_{s1}} \end{pmatrix} & \bar{\varepsilon}_{s2} &= \begin{pmatrix} \varepsilon_{s2} \\ s_{\varepsilon_{s2}} \end{pmatrix} \\ \bar{\varepsilon} &= \begin{pmatrix} \varepsilon_1 \\ \varepsilon_2 \end{pmatrix} \end{aligned} \quad (39)$$

Elements A_x , A_y , A_ϕ , A_δ , $A_{\varepsilon_{p1}}$, $A_{\varepsilon_{p2}}$, $B_x^{\varepsilon_{p1}}(t)$, $B_x^{\varepsilon_{p2}}(t)$, $B_y^{\varepsilon_{p1}}$, $B_y^{\varepsilon_{p2}}$, $B_\phi^{\varepsilon_{p1}}$ and $B_\phi^{\varepsilon_{p2}}$ of matrix $G(t)$ are defined as in Eq. (25), matrices $A_{\varepsilon_{s1}}$, $A_{\varepsilon_{s2}}$ and A_ε are given by

$$\begin{aligned} A_{\varepsilon_{s1}} &= \begin{pmatrix} -\lambda_{\varepsilon_{s1}} & 1 \\ 0 & -g_{14,14} \end{pmatrix} & A_{\varepsilon_{s2}} &= \begin{pmatrix} -\lambda_{\varepsilon_{s2}} & 1 \\ 0 & -g_{16,16} \end{pmatrix} \\ A_\varepsilon &= \begin{pmatrix} -\lambda_{\varepsilon_1} & 0 \\ g_{18,17} & -\lambda_{\varepsilon_2} \end{pmatrix} \end{aligned} \quad (40)$$

and the remaining components of $G(t)$ are defined as

$$\begin{aligned} B_x^{\varepsilon_{s1}} &= \begin{pmatrix} 0 & 0 \\ g_{2,13} & -v \end{pmatrix} & B_x^{\varepsilon} &= \begin{pmatrix} 0 & 0 \\ -v & 0 \end{pmatrix} \\ B_\delta^{\varepsilon_{s1}} &= \begin{pmatrix} 0 & 0 \\ g_{8,13} & v \end{pmatrix} & B_\delta^{\varepsilon_{s2}} &= \begin{pmatrix} 0 & 0 \\ g_{8,15} & -v \end{pmatrix} \\ B_\delta^{\varepsilon} &= \begin{pmatrix} 0 & 0 \\ v & -v \end{pmatrix} & B_\varepsilon^x &= \begin{pmatrix} g_{17,1} & g_{17,2} \\ g_{18,1} & g_{18,2} \end{pmatrix} \\ B_\varepsilon^\phi(t) &= \begin{pmatrix} g_{17,5} & g_{17,6} \\ g_{18,5} & g_{18,6} \end{pmatrix} & B_\varepsilon^\delta &= \begin{pmatrix} 0 & 0 \\ g_{18,7} & g_{18,8} \end{pmatrix} \\ B_\varepsilon^{\varepsilon_{p1}}(t) &= \begin{pmatrix} g_{17,9} & g_{17,10} \\ g_{18,9} & g_{18,10} \end{pmatrix} & B_\varepsilon^{\varepsilon_{p2}}(t) &= \begin{pmatrix} g_{17,11} & g_{17,12} \\ g_{18,11} & g_{18,12} \end{pmatrix} \\ B_\varepsilon^{\varepsilon_{s1}} &= \begin{pmatrix} g_{17,13} & g_{17,14} \\ g_{18,13} & g_{18,14} \end{pmatrix} & B_\varepsilon^{\varepsilon_{s2}} &= \begin{pmatrix} 0 & 0 \\ g_{18,15} & g_{18,16} \end{pmatrix} \end{aligned} \quad (41)$$

The elements, $g_{i,j}$, of the matrices defined above depend on system parameters and the controller gains. As in the simplified system, we can break down Eq. (36) into

$$\begin{aligned} \dot{\bar{x}} &= A_x \bar{x} + B_x^{\varepsilon_{p1}}(t) \bar{\varepsilon}_{p1} + B_x^{\varepsilon_{p2}}(t) \bar{\varepsilon}_{p2} + B_x^{\varepsilon_{s1}} \bar{\varepsilon}_{s1} + B_x^{\varepsilon} \bar{\varepsilon} \\ \dot{\bar{y}} &= A_y \bar{y} + B_y^{\varepsilon_{p1}} \bar{\varepsilon}_{p1} + B_y^{\varepsilon_{p2}} \bar{\varepsilon}_{p2} \\ \dot{\bar{\phi}} &= A_\phi \bar{\phi} + B_\phi^{\varepsilon_{p1}} \bar{\varepsilon}_{p1} + B_\phi^{\varepsilon_{p2}} \bar{\varepsilon}_{p2} \\ \dot{\bar{\delta}} &= A_\delta \bar{\delta} + B_\delta^{\varepsilon_{s1}} \bar{\varepsilon}_{s1} + B_\delta^{\varepsilon_{s2}} \bar{\varepsilon}_{s2} + B_\delta^{\varepsilon} \bar{\varepsilon} \\ \dot{\bar{\varepsilon}}_{p1} &= A_{\varepsilon_{p1}} \bar{\varepsilon}_{p1} \\ \dot{\bar{\varepsilon}}_{p2} &= A_{\varepsilon_{p2}} \bar{\varepsilon}_{p2} \\ \dot{\bar{\varepsilon}}_{s1} &= A_{\varepsilon_{s1}} \bar{\varepsilon}_{s1} \\ \dot{\bar{\varepsilon}}_{s2} &= A_{\varepsilon_{s2}} \bar{\varepsilon}_{s2} \\ \dot{\bar{\varepsilon}} &= A_\varepsilon \bar{\varepsilon} + B_\varepsilon^x \bar{x} + B_\varepsilon^\phi(t) \bar{\phi} + B_\varepsilon^\delta \bar{\delta} + B_\varepsilon^{\varepsilon_{p1}}(t) \bar{\varepsilon}_{p1} + B_\varepsilon^{\varepsilon_{p2}}(t) \bar{\varepsilon}_{p2} \\ &\quad + B_\varepsilon^{\varepsilon_{s1}} \bar{\varepsilon}_{s1} + B_\varepsilon^{\varepsilon_{s2}} \bar{\varepsilon}_{s2} \end{aligned} \quad (42)$$

We can see from Eq. (42) that we can easily solve for ε_{pi} , ε_{si} , ($i = 1, 2$):

$$\begin{aligned} \bar{\varepsilon}_{p1}(t) &= e^{A_{\varepsilon_{p1}} t} \bar{\varepsilon}_{p1}(0) \\ \bar{\varepsilon}_{p2}(t) &= e^{A_{\varepsilon_{p2}} t} \bar{\varepsilon}_{p2}(0) \\ \bar{\varepsilon}_{s1}(t) &= e^{A_{\varepsilon_{s1}} t} \bar{\varepsilon}_{s1}(0) \\ \bar{\varepsilon}_{s2}(t) &= e^{A_{\varepsilon_{s2}} t} \bar{\varepsilon}_{s2}(0) \end{aligned} \quad (43)$$

The expressions for $\bar{x}(t)$, $\bar{y}(t)$, $\bar{\phi}(t)$, $\bar{\delta}(t)$, and $\bar{\varepsilon}(t)$ can be obtained

from Eq. (42) and (43):

$$\begin{aligned}
\bar{x}(t) &= e^{A_x t} \bar{x}(0) + \int_0^t e^{A_x(t-\tau)} B_x^{\varepsilon_{p1}}(\tau) e^{A_{\varepsilon_{p1}} \tau} d\tau \bar{\varepsilon}_{p1}(0) \\
&+ \int_0^t e^{A_x(t-\tau)} B_x^{\varepsilon_{p2}}(\tau) e^{A_{\varepsilon_{p2}} \tau} d\tau \bar{\varepsilon}_{p2}(0) + \int_0^t e^{A_x(t-\tau)} B_x^{\varepsilon_{s1}} e^{A_{\varepsilon_{s1}} \tau} d\tau \bar{\varepsilon}_{s1}(0) \\
&+ \int_0^t e^{A_x(t-\tau)} B_x^{\varepsilon_{s2}} e^{A_{\varepsilon_{s2}} \tau} d\tau \bar{\varepsilon}_{s2}(0) + \int_0^t e^{A_x(t-\tau)} B_x^{\varepsilon} \bar{\varepsilon}(\tau) d\tau \\
\bar{y}(t) &= e^{A_y t} \bar{y}(0) + \int_0^t e^{A_y(t-\tau)} B_y^{\varepsilon_{p1}} e^{A_{\varepsilon_{p1}} \tau} d\tau \bar{\varepsilon}_{p1}(0) \\
&+ \int_0^t e^{A_y(t-\tau)} B_y^{\varepsilon_{p2}} e^{A_{\varepsilon_{p2}} \tau} d\tau \bar{\varepsilon}_{p2}(0) \\
\bar{\phi}(t) &= e^{A_\phi t} \bar{\phi}(0) + \int_0^t e^{A_\phi(t-\tau)} B_\phi^{\varepsilon_{p1}} e^{A_{\varepsilon_{p1}} \tau} d\tau \bar{\varepsilon}_{p1}(0) \\
&+ \int_0^t e^{A_\phi(t-\tau)} B_\phi^{\varepsilon_{p2}} e^{A_{\varepsilon_{p2}} \tau} d\tau \bar{\varepsilon}_{p2}(0) \\
\bar{\delta}(t) &= e^{A_\delta t} \bar{\delta}(0) + \int_0^t e^{A_\delta(t-\tau)} B_\delta^{\varepsilon_{s1}} e^{A_{\varepsilon_{s1}} \tau} d\tau \bar{\varepsilon}_{s1}(0) \\
&+ \int_0^t e^{A_\delta(t-\tau)} B_\delta^{\varepsilon_{s2}} e^{A_{\varepsilon_{s2}} \tau} d\tau \bar{\varepsilon}_{s2}(0) + \int_0^t e^{A_\delta(t-\tau)} B_\delta^{\varepsilon} \bar{\varepsilon}(\tau) d\tau \\
\bar{\varepsilon}(t) &= e^{A_\varepsilon t} \bar{\varepsilon}(0) + \int_0^t e^{A_\varepsilon(t-\tau)} B_\varepsilon^x \bar{x}(\tau) d\tau \\
&+ \int_0^t e^{A_\varepsilon(t-\tau)} B_\varepsilon^\phi(\tau) \bar{\phi}(\tau) d\tau + \int_0^t e^{A_\varepsilon(t-\tau)} B_\varepsilon^\delta \bar{\delta}(\tau) d\tau \\
&+ \int_0^t e^{A_\varepsilon(t-\tau)} B_\varepsilon^{\varepsilon_{p1}}(\tau) e^{A_{\varepsilon_{p1}} \tau} d\tau \bar{\varepsilon}_{p1}(0) + \int_0^t e^{A_\varepsilon(t-\tau)} B_\varepsilon^{\varepsilon_{p2}}(\tau) e^{A_{\varepsilon_{p2}} \tau} d\tau \bar{\varepsilon}_{p2}(0) \\
&+ \int_0^t e^{A_\varepsilon(t-\tau)} B_\varepsilon^{\varepsilon_{s1}} e^{A_{\varepsilon_{s1}} \tau} d\tau \bar{\varepsilon}_{s1}(0) + \int_0^t e^{A_\varepsilon(t-\tau)} B_\varepsilon^{\varepsilon_{s2}} e^{A_{\varepsilon_{s2}} \tau} d\tau \bar{\varepsilon}_{s2}(0)
\end{aligned} \tag{44}$$

As in the case of the simplified system, we can see from Eqs. (25), (40), (43), and (44) that, by proper selection of the controller gains, we can make matrices A_x , A_y , A_ϕ , A_δ , $A_{\varepsilon_{p1}}$, $A_{\varepsilon_{p2}}$, $A_{\varepsilon_{s1}}$, $A_{\varepsilon_{s2}}$, and A_ε Hurwitz, and thus we can make the solutions $\bar{x}(t)$, $\bar{y}(t)$, $\bar{\phi}(t)$, $\bar{\delta}(t)$, $\bar{\varepsilon}_{p1}(t)$, $\bar{\varepsilon}_{p2}(t)$, $\bar{\varepsilon}_{s1}(t)$, $\bar{\varepsilon}_{s2}(t)$, and $\bar{\varepsilon}(t)$ converge.

6.3 Controller Design Methodology

Let us first assume the same control specifications as in Section 5.3. Then, just as in the case of the simplified system and based on the expressions in Eqs. (43) and (44), we can develop a procedure to calculate the controller gains for a sheet of finite dimensions moving at a pre-specified nominal longitudinal velocity with some given initial and final state errors. This time, however, the gains corresponding to $\bar{x}(t)$, $\bar{\delta}(t)$, and $\bar{\varepsilon}(t)$ cannot be obtained directly, since the expressions for $\bar{x}(t)$ and $\bar{\delta}(t)$ depend on $\bar{\varepsilon}(t)$ and vice versa. Thus, we need to use the following iterative procedure.

- i. Determine gains $(\lambda_{\varepsilon_{p1}}, \eta_{p1})$, $(\lambda_{\varepsilon_{p2}}, \eta_{p2})$, $(\lambda_{\varepsilon_{s1}}, \gamma_{s1})$, and $(\lambda_{\varepsilon_{s2}}, \gamma_{s2})$ from Eqs. (43).
- ii. Once the gains from step (i) have been obtained, determine gains (λ_y, K_y) , and (λ_ϕ, K_ϕ) from the second and third expressions of Eqs. (44).
- iii. Using the gains (λ_x, K_x) and $(\lambda_\delta, K_\delta)$ obtained in Section 5.3 as initial guesses, determine gains (τ_1, τ_2) from the last expression in Eqs. (44).
- iv. Check that the initial guesses for gains (λ_x, K_x) and $(\lambda_\delta, K_\delta)$ are fine by using the first and fourth expressions in Eqs. (44).
- v. Iterate between steps (iii) and (iv) if necessary.

As stated in step (iii), even though this procedure requires some iteration, it should be noted that the results from the controller design methodology obtained for the simplified system (Section

5.3) can be used as initial points for the controller implemented experimentally. Furthermore, in most cases we only need one or two iterations before we arrive to the right controller gains for the desired specifications.

6.4 Simulation and Experimental Results

In order to determine the efficacy of the controller developed, we again have performed simulation tests for a letter-sized sheet moving at the same nominal longitudinal velocity of 0.5m/s from the initial to the final state errors shown in Table 1. Based on the initial and final errors shown in Table 1 and the methodology presented in Section 6.3 with the initial guesses for (λ_x, K_x) and $(\lambda_\delta, K_\delta)$ from Section 5.3, the following controller gains were obtained:

$$\begin{aligned}
(\lambda_x, K_x) &= (80, 4.5); & (\lambda_y, K_y) &= (80, 8.0) \\
(\lambda_\phi, K_\phi) &= (80, 4.9); & (\lambda_\delta, K_\delta) &= (95, 4.0) \\
(\lambda_{\varepsilon_{p1}}, \eta_{p1}) &= (100, 0.26); & (\lambda_{\varepsilon_{p2}}, \eta_{p2}) &= (100, 0.26) \\
(\lambda_{\varepsilon_{s1}}, \gamma_{s1}) &= (100, 9.31); & (\lambda_{\varepsilon_{s2}}, \gamma_{s2}) &= (100, 9.31) \\
(\tau_1, \tau_2) &= (0.0042, 0.0013)
\end{aligned}$$

Note that the controller gains obtained are similar to those in Section 5.4, which shows that we do not need to perform too many iterations before arriving to an appropriate set of gains. We can see in Fig. 9 that the controller effectively corrects the position of the sheet within the pre-specified allowable time of 0.42 seconds.

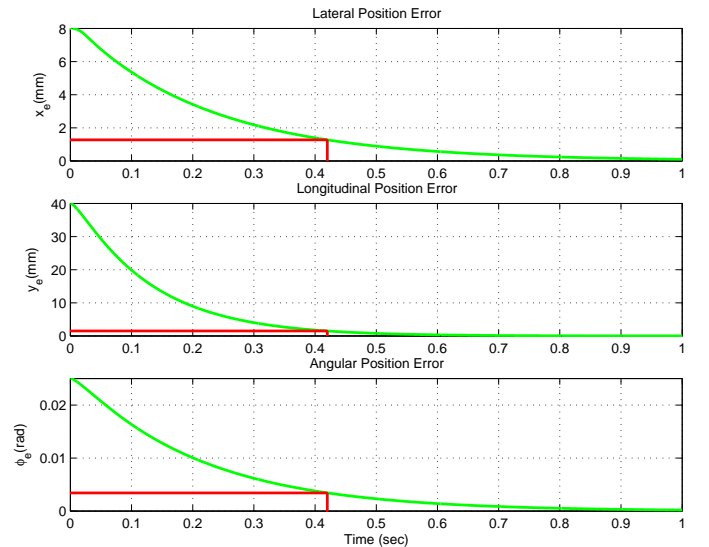


Figure 9. Simulation Results for the System Implemented

Initial Errors	Final Errors
$ \tilde{x}(0) \leq 0.004 \text{ m}$	$ \tilde{x}(T) \leq 0.00026 \text{ m}$
$ \tilde{y}(0) \leq 0.0074 \text{ m}$	$ \tilde{y}(T) \leq 0.0005 \text{ m}$
$ \tilde{\phi}(0) \leq 0.025 \text{ rad}$	$ \tilde{\phi}(T) \leq 0.001 \text{ rad}$
$ \tilde{\delta}(0) \leq 0.0001 \text{ m}$	$ \tilde{\delta}(T) \leq 0.00002 \text{ m}$

Table 2. Initial and Final State Errors for the Experimental Test

Furthermore, we have also performed experimental tests in the system shown in Fig. 3. It should be noticed, however, that the actual experimental fixture cannot handle initial errors as large as those in Table 1 due to limitations in the setup design (size of the laser sensors for lateral and angular measurements in Fig. 1). Therefore, based on the methodology presented in Section 6.3 and the initial and final errors shown in Table 2, the following controller gains were obtained:

$$\begin{aligned}
(\lambda_x, K_x) &= (80, 12.5); & (\lambda_y, K_y) &= (80, 13.2) \\
(\lambda_\phi, K_\phi) &= (80, 11.2); & (\lambda_\delta, K_\delta) &= (80, 7.9) \\
(\lambda_{\epsilon_{p1}}, \eta_{p1}) &= (100, 0.26); & (\lambda_{\epsilon_{p2}}, \eta_{p2}) &= (100, 0.26) \\
(\lambda_{\epsilon_{s1}}, \gamma_{s1}) &= (100, 9.31); & (\lambda_{\epsilon_{s2}}, \gamma_{s2}) &= (100, 9.31) \\
(\tau_1, \tau_2) &= (0.0042, 0.0013); & &
\end{aligned}$$

As shown in Fig. 10, using these gains we were able to correct the sheet's position in about 0.3 seconds. Note that the longitudinal position increases constantly because the sheet moves in the longitudinal direction at all times. Here we can also see the correction made by the open-loop observer on the longitudinal position once the sheet arrives to the second optical sensor (see Fig. 1) at about 0.09 seconds. The small discrepancies observed between simulation and experimental results can be attributed to sensor noise and accuracy.

7 CONCLUSION

In this paper we have presented an innovative design that permits a swifter correction of lateral, longitudinal and angular position errors in a paper path control system for xerographic and printing devices. This mechanism accomplished this task by having steer-able nips.

In order to correct the sheet position errors we have used a control based on state feedback linearization [3] with the addition of internal loops for the control of the process direction velocity and steering position of the rollers.

In addition, not only have we provided a convergence analysis for the controller implemented, but also we have described a design methodology to determine its gains. Even though this methodology requires some iteration, we can use the controller gains obtained for a simplified system as initial points.

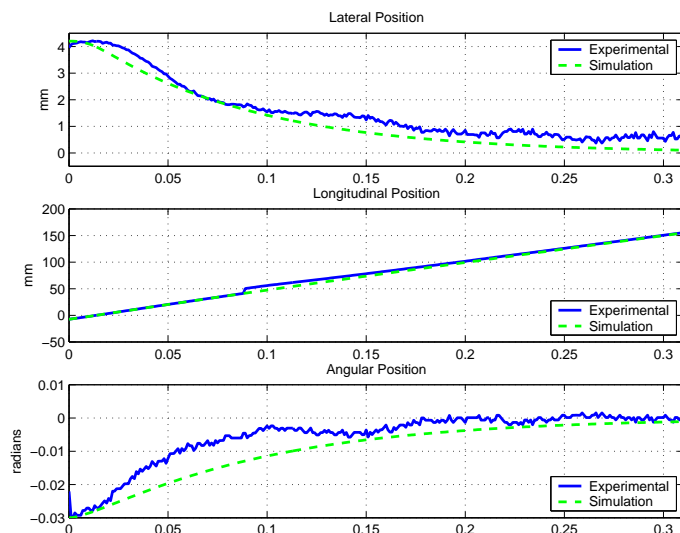


Figure 10. Experimental and Simulation Results

Simulation and experimental results show that by using the controller gains obtained from the methodology previously mentioned, it is possible to drive a sheet from an initial state with nonzero longitudinal velocity to a final state also with nonzero longitudinal velocity in a very short time.

8 ACKNOWLEDGEMENTS

This work was supported by the National Science Foundation under Grant CMS 0301719 and by financial support and collaboration from Xerox Corporation. In particular, the authors thank Dr. Martin Krucinski for his numerous critical remarks.

REFERENCES

- [1] Xiaoping Yun and N. Sarkar. Dynamic feedback control of vehicles with two steerable wheels. In *1996 IEEE International Conference on Robotics and Automation*, pages 3105–3110, 1996.
- [2] Rene Sanchez, Roberto Horowitz, and Masayoshi Tomizuka. Paper sheet control using steerable nips. In *2004 American Control Conference Proceedings*, pages 482–487, Boston, Massachusetts, June 30–July 2 2004.
- [3] S. S. Sastry. *Nonlinear Systems : Analysis, Stability, and Control*. Springer, 1999.
- [4] Rene Sanchez, Edgar Ergueta, Benjamin Fine, Roberto Horowitz, Masayoshi Tomizuka, and Martin Krucinskić. A mechatronic approach to full sheet control using steer-able nips. In *4th IFAC Symposium in Mechatronic Systems*, Heidelberg, Germany, 12– 15 2006.
- [5] J.-J. E. Slotine and W. Li. *Applied Nonlinear Control*. Prentice Hall, Inc., N.J., 1991.